CALCULATION OF PITCH-LINK LOADS IN DEEP STALL USING STATE-OF-THE-ART METHODOLOGY

Jing G. Yen and Mithat Yuce
Bell Helicopter Textron, Inc.
Fort Worth, Texas U.S.A.

Abstract

Pitch-link loads for bearingless rotors in deep stall are calculated using a unified state-of-the-art methodology. The methodology includes a modern free wake model for blade–vortex interaction, advanced unsteady-aerodynamic and dynamic-stall models, and a state-of-the-art rotor dynamics modeling for redundant load paths on bearingless rotors. Validation of the methodology is briefly discussed. Correlations of theory with measured pitch-link loads are presented. The measured data are from wind tunnel tests of two 1/5 Mach-scaled rotor models with the same bearingless hub but with blades having different torsional rigidities, and from flight tests of three full-scale bearingless rotors with different torsional frequencies and solidities. Data are presented as functions of advance ratios and rotor thrust coefficients, and also in time-history waveforms. Effects of blade–vortex interaction, blade torsional stiffness, unsteady aerodynamics, and solidity on pitch-link loads in deep stall are discussed.

Notation

c	thrust-weighted chord, ft
C_d	drag coefficient
C_ℓ	lift coefficient
C_m	moment coefficient
C_T	rotor thrust coefficient, $T/[\pi R^2 \rho (R\Omega)^2]$
K	reduced frequency of airfoil oscillation
M	Mach number
N	number of blades
R	rotor radius, ft
T	rotor thrust, lb
V	airspeed, ft/sec
α	angle of attack, deg
μ	advance ratio, $V/R\Omega$
ρ	air density, slug/ft^3
σ	rotor solidity, $Nc/\pi R$
Ψ	blade azimuth, deg
Ω	rotor speed, rad/sec
ω	oscillating frequency, rad/sec
ω_n	first torsion natural frequency, per rev

Introduction

A reliable prediction of amplitude and waveform of pitch-link loads at high advance ratios and high load factors has been a challenge for dynamics engineers. It is a well-known fact that proper representation of blade torsional rigidity and control system stiffness is important in such predictions. They directly affect the rotor torsional natural frequency and, hence, the pitch-link-load waveform, particularly in deep stall. High pitch-link loads in deep stall result from an aeroelastic, self-excited, blade pitching motion precipitated by repeated submersion of a large portion of the blade into and out of stall. This phenomenon is the classical stall flutter. In addition to an accurate rotor dynamics representation, a reliable prediction of stall flutter depends on adequate modeling of wake-induced inflows and dynamic stall effects. A detailed investigation of these effects was conducted by Tarzanin (Ref 1). Based on analytical investigation and limited correlation, Tarzanin concluded that the magnitudes of pitch-link loads resulting from stall flutter were a function of torsional natural frequency, that inclusions of wake-induced inflows were essential to a better prediction of pitch-link-load magnitudes, and that the dynamic-stall delay was the fundamental source of stall flutter.

Significant progress has been made in recent years in the development of free wake models to account for wake-induced inflow due to blade–vortex interaction (Refs 2 and 3). Extensive work has also been done on the correlation of theoretical blade–vortex interaction airloads with measured airloads (e.g., Refs 4, 5, and 6). The results are encouraging.

Classical unsteady-aerodynamic and dynamic-stall theories were developed in the early 1970s (Refs 1, 7, and 8) and have been used routinely at Bell. Gangwani developed an empirical model for dynamic stall (Ref 9) which he used for a limited correlation with flight test rotor loads (Ref 10). A semi-empirical dynamic stall model developed by ONERA (Ref 11) was used to make a correlation with flight test blade loads obtained from an Aerospatiale Gazelle SA 349/2 helicopter (Ref 12). As reported in Ref 12, the predicted time history of the pitch-link loads was poor and the most discrepancy was found in the retreating blade. A more recent formulation of semi-empirical unsteady-aerodynamic and dynamic-stall

modeling using the indicial method was developed by Leishman and Beddoes (Refs 13 and 14). Comparisons of the theory with two-dimensional oscillating airfoil data on section lift force, pressure drag, and pitching moment hysteresis in deep dynamic stall showed good agreement. However, no rotor loads data have been found in the literature using the Leishman/Beddoes dynamic-stall modeling.

Bell Helicopter Textron, Inc. has been developing COPTER, a second-generation global rotorcraft flight-simulation program (Ref 15), since 1979. COPTER (COmprehensive Program for Theoretical Evaluation of Rotorcraft) was developed from C81 (Ref 16) by restructuring and modularizing. As did C81, COPTER analysis capabilities include rotor loads, forward flight performance, handling qualities, vibration, and aeroelastic stability. Drees inflow model (Ref 17) and BUNS unsteady aerodynamics (lift from Ref 1, drag from Ref 7, and moment from Ref 8) were used successfully in C81 and are also available in COPTER. New technology modules recently implemented in COPTER include the Johnson free wake model (Ref 3) and Leishman unsteady aerodynamics (Ref 13).

The rotor dynamics are represented by 20 elastic modes obtained from Myklestad analysis (Ref 18). The redundant load path of a bearingless hub is properly treated in the Myklestad analysis.

This paper presents correlations of pitch-link loads for bearingless rotors in deep stall using COPTER with state-of-the-art methodology. The measured data were obtained from wind tunnel tests of two bearingless rotor models as well as flight tests of three full-scale bearingless rotors with different torsional frequencies and solidity. The present paper complements the previous work by Tarzanin (Ref 1) in that the effect of blade–vortex interaction on pitch-link loads in deep stall is re-examined using a modern free wake model, that the effect of rotor torsional frequency on the magnitude of stall-flutter pitch-link loads is reviewed, and that the effect of the dynamic-stall model of Leishman is compared with that of BUNS on pitch-link-load waveforms.

Validation of Methodology

The unified state-of-the-art methodology available in COPTER for rotor loads analysis includes the Johnson free wake model (Ref 3), BUNS (Refs 1, 7, and 8) and Leishman (Ref 13) unsteady aerodynamics models, and Myklestad rotor dynamics analysis (Ref 18). Before the correlation of pitch-link loads in deep stall is presented, a brief discussion of the methodology is given.

Airloads Correlations

An experiment was conducted using a pressure-instrumented rotor in conjunction with a laser velocimeter system to measure airloads and rotor wake structure at high advance ratios (Ref 19). The model was a 1/5 Mach scale of the Bell Advanced Light Rotor (ALR), a four-bladed bearingless soft-in-plane rotor. The model was tested at the NASA Langley 14- by 22-ft subsonic wind tunnel in May 1989. Ninety-two pressure transducers were installed on two opposite blades at five spanwise locations: 0.69R, 0.73R, 0.81R, 0.87R, and 0.96R. The experimental vibratory airloads were obtained by integrating the individual pressures.

The measured blade sectional normal forces at 0.96R were compared with predictions using the Johnson free wake model in the COPTER rotor loads analysis. The free wake option used in this paper consisted of two circulation peaks, first-order lifting line theory, and 0.04R vortex core size. Results are shown in Figs 1(a) and 1(b) for $\mu = 0.20$, $C_T/\sigma = 0.117$ and $\mu = 0.37$, $C_T/\sigma = 0.085$, respectively. The rotor thrust coefficient, C_T/σ, for the ALR at 1g thrust is 0.055. At $\mu = 0.20$, the measured data show a vortex interaction on the retreating side. At $\mu = 0.37$, the lift at the advancing blade tip becomes negative to maintain a roll-moment trim. The COPTER predictions with the free wake model follow the same trend as the experimental data.

Correlation of blade aerodynamic pitching moments about the quarter-chord at 0.87R is shown in Fig 2. The theory was based on the Johnson free wake model and BUNS unsteady aerodynamics. At $\mu = 0.20$, $C_T/\sigma = 0.117$, both the measured data and the theory show an on-set dynamic stall near an azimuth of 240°. At $\mu = 0.37$, $C_T/\sigma = 0.085$, a strong retreating blade stall is predicted by the theory. A much milder stall, however, is shown by the measured data. As depicted, the level of correlation for the pitching moment is not as good as that for the normal force. Further study of the effect of aerodynamic pitching moment on pitch-link loads in deep stall revealed that an initial nose-down disturbance in the pitching moment due to stall is essential for the pitch-link-loads response on the retreating blade side and that a major portion of the pitch-link-loads waveform is dominated by the blade yoke torsional stiffness and tennis racket moment. Hence, the less-than-desired correlation level in aerodynamic pitching moment depicted in Fig 2 does not significantly degrade the pitch-link-loads prediction. This is evident from the loads correlations shown later in this paper.

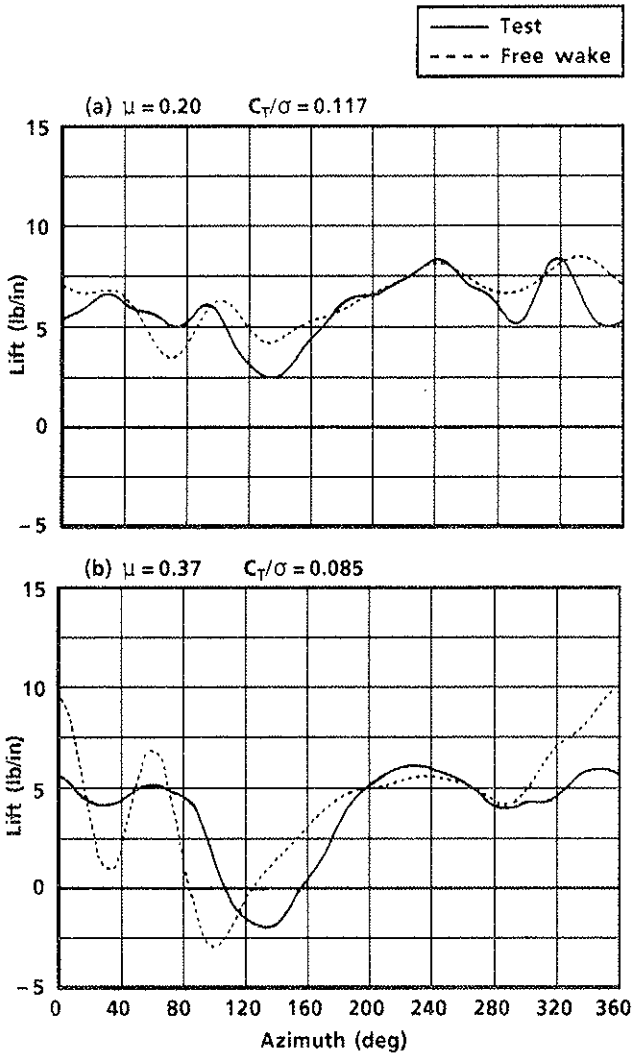

Fig. 1. Correlation of measured airloads at 0.96R on pressure-instrumented rotor with theory using free wake.

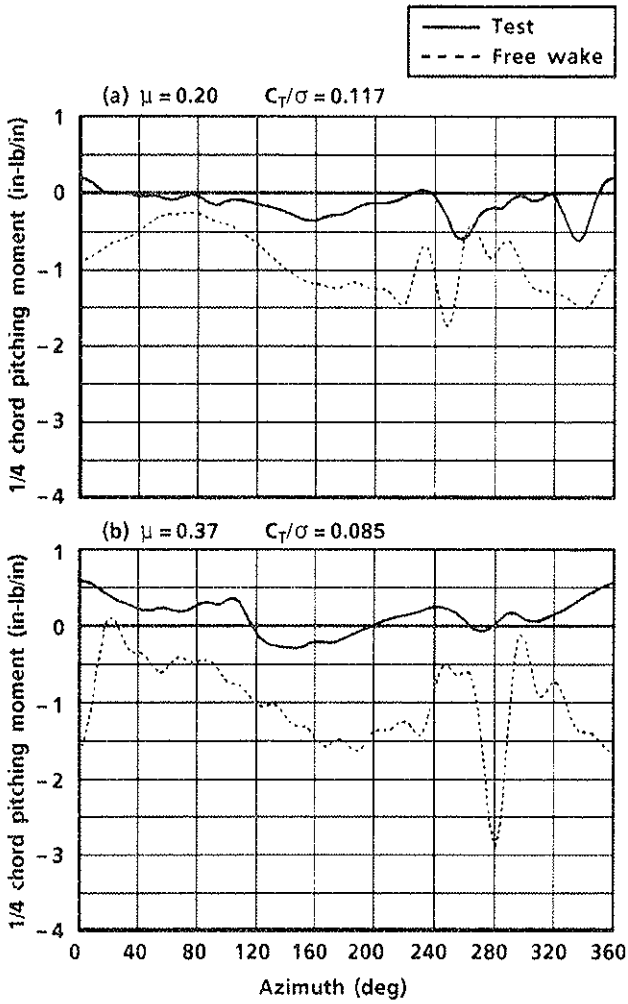

Fig. 2. Correlation of measured pitching moments at 0.87R on pressure-instrumented rotor with theory using free wake.

Unsteady Aerodynamics

The BUNS unsteady aerodynamics was implemented in C81 in the early 1970s and has been used extensively at Bell for rotor loads analysis. The theoretical formulations for lift, drag, and moment coefficients of BUNS were obtained from Refs 1, 7, and 8, respectively. Correlations of the theories with two-dimensional oscillating airfoil data were good, according to these references.

The aerodynamic forces and moments calculated using the Leishman unsteady aerodynamics model were compared with McCroskey's two-dimensional airfoil data (Ref 20) for a NACA 0012 airfoil at a Mach number of 0.3 and a reduced frequency of 0.1. The McCroskey oscillating airfoil was constrained to oscillate in such a way that a 10° sinusoidal motion was superimposed on a 10° mean angle of attack. Results of the comparison are shown in Fig 3. Good correlation is evident.

Bearingless Rotor Dynamics

The ability of the Myklestad analysis (Ref 18) to model a bearingless rotor is demonstrated by the frequency correlation shown in Fig 4. The bearingless rotor used for the demonstration is the Bell ALR (Ref 21). Results show good correlation in frequencies up to 7/rev, including that of the first torsion mode.

Model Rotor Correlation

A 1/5 Mach-scaled baseline ALR was tested for high advance ratios and high thrust levels in the 8.5- by 12-ft low-speed wind tunnel of McDonnell Douglas Aircraft Corporation (MCAIR) in November 1988.

To evaluate the effect of blade torsional stiffness on pitch-link loads, a 1/5 Mach-scaled torsionally stiff rotor was designed, fabricated, and tested in

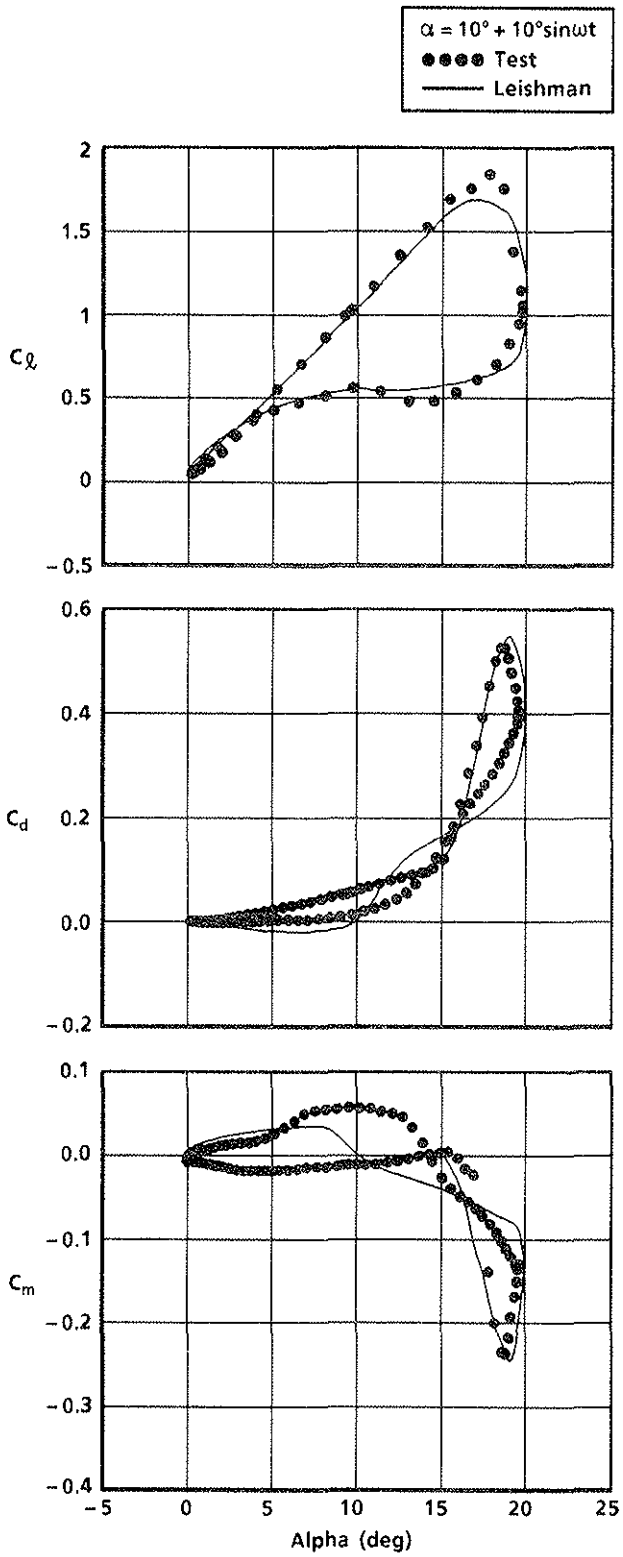

Fig. 3. Correlation of NACA 0012 forces and moments data during strong dynamic stall with theory using Leishman for M = 0.302 and K = 0.0963.

the MCAIR wind tunnel in August 1989. The torsionally stiff rotor blades were designed to match the beamwise and chordwise stiffness and inertial properties of the baseline blades but have

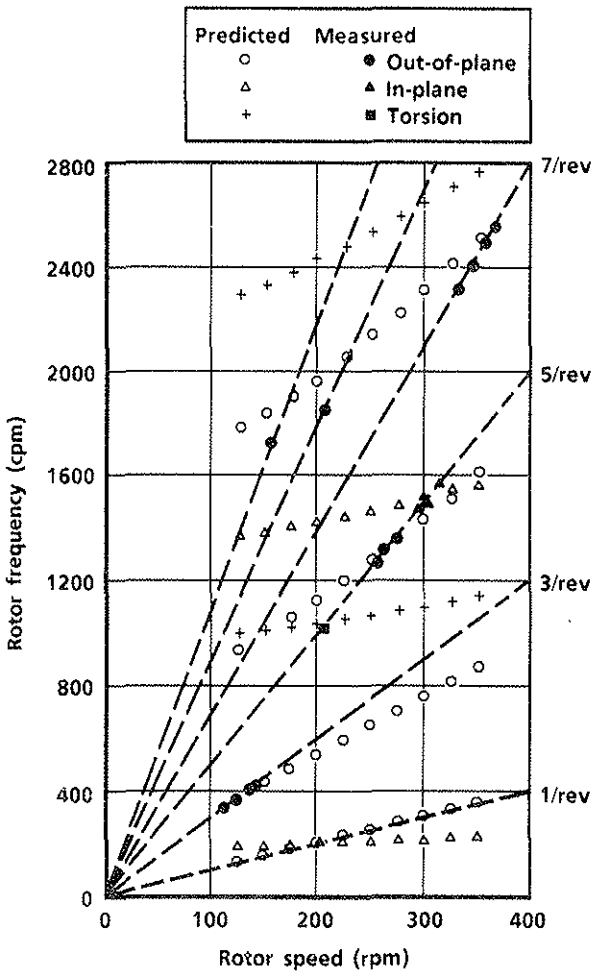

Fig. 4. Correlation of analytical and measured ALR cyclic mode frequencies.

four times the torsional stiffness. The pitch-link static stiffness was measured. Frequencies of the first three cyclic modes and the first torsion mode of the torsionally stiff rotor are compared with those of the baseline rotor in Table 1.

Analytical investigations of the effects of blade–vortex interaction, torsional stiffness, and Leishman unsteady aerodynamics on pitch-link-load predictions in deep stall were conducted using the loads data measured on these two model rotors. The results are discussed below.

Effect of Blade–Vortex Interaction on Pitch-Link Loads

Both Johnson's free wake and Drees inflow models were used to compute oscillatory pitch-link loads for the baseline rotor. BUNS unsteady aerodynamics was used in both cases. The resulting loads are shown in Fig 5 as functions of rotor thrust coefficient for $\mu = 0.25, 0.35$, and 0.39. The measured loads are shown for comparison. The plots indicate that trends manifested by the free

TABLE 1. ROTOR CYCLIC MODE FREQUENCIES (PER REV)

Mode	1/5 Mach-Scaled ALR Baseline	Torsionally Stiff
1st in-plane	0.60	0.61
1st out-of-plane	1.03	1.03
2nd out-of-plane	2.59	2.58
1st torsion	3.21	4.88

Mode	Full-Scale ALR	680	4BW
1st in-plane	0.68	0.71	0.73
1st out-of-plane	1.02	1.02	1.02
2nd out-of-plane	2.49	2.45	2.48
1st torsion	3.29	5.14	3.35

wake data correlate better than those by the Drees inflow data. The benefit of using the free wake model is particularly appreciated in deep stall, i.e., at higher μ and C_T/σ combinations.

Correlations of measured and computed pitch-link-load waveforms are shown in Fig 6 for the same advance ratios as Fig 5 and at the maximum C_T/σ values obtained by the analysis. The theoretical loads were calculated using the free wake model. Good agreement between the measured and theoretical data is evident.

Figs 7 and 8 show the same correlations for the torsionally stiff blades as Figs 5 and 6 do for the baseline blades. The plots for the torsionally stiff blades indicate that pitch-link-loads prediction with the free wake model correlates better with the test data than the Drees inflow model (Fig 7) and that correlation of the waveform (Fig 8) is not as good as that for the baseline rotor.

As shown in Figs 5 and 7, there is a distinct difference in trends between the results of the Johnson free wake model and the Drees inflow model. A close examination of the analytical data revealed that the influence of the blade–vortex interaction captured only by the free wake model was responsible for the better correlation results.

Shown in Fig 9 are time histories of the induced velocity as computed by the Johnson free wake model for $\mu = 0.35$, $C_T/\sigma = 0.11$ at 0.75R, 0.83R, 0.87R, 0.91R, and 0.95R on the torsionally stiff blades. Strong blade–vortex interaction is seen at all these blade stations. The angle of attack at each of these stations is depicted in Fig 10. Notice that the whole outboard region of the blade stalls simultaneously when the blade is near 270° azimuth and that the dynamic-stall delay boundary (rate of change of the angle of attack equals zero) is found at 275° azimuth for the outboard 20% radius. The simultaneous stall and dynamic-stall delay were caused by the blade–vortex interaction (Fig 9). This simultaneous stall over the portion of the blade carrying the large airloading accounts for the initial nose-down stall spike in the pitch-link-load waveform (Fig 8). The negative pitch damping and elastic blade twist lead to the subsequent stall flutter spikes until angles of attack insufficient for stall are obtained and positive damping takes over.

Effect of Blade Torsional Stiffness on Pitch-Link Loads

As discussed earlier in this paper, the blade torsional stiffness of the torsionally stiff rotor was four times that of the baseline rotor. The resulting first-torsion frequencies are 4.88/rev and 3.21/rev, respectively, as shown in Table 1. Measured pitch-link loads for the torsionally stiff and baseline rotors are shown in Fig 11 for comparison. Notice that there is no significant difference in pitch-link loads due to blade torsional stiffness. Computed pitch-link loads for both rotors are shown in Fig 12. Again, the difference in blade torsional stiffness has no significant effect on the loads.

The effect of blade torsional stiffness on pitch-link loads was further studied using a simple analytical model. This model included the following:

1. The blade aerodynamic loading was initiated by a step input in C_m of –0.1 on the outboard 40% radius between azimuth angles of 265° and 30°. This is depicted in Fig 13.

2. The blade dynamics was represented by the first torsion mode. A zero modal damping was assumed where the negative pitching moment was applied. A modal damping of 20% was used where the pitching moment became zero.

Three rotors with different blade torsional stiffnesses were used for this study. The frequencies of the first torsion mode were 3.35/rev, 4.7/rev, and 6.7/rev. In a forward flight condition, an aerodynamic impulse pitching moment was computed using the step C_m input (Fig 13). Computed pitch-link-load responses of the three rotors to the same aerodynamic impulse pitching moment excitation are shown in Fig 13. Fig 14 shows the harmonic decomposition of the three pitch-link-load

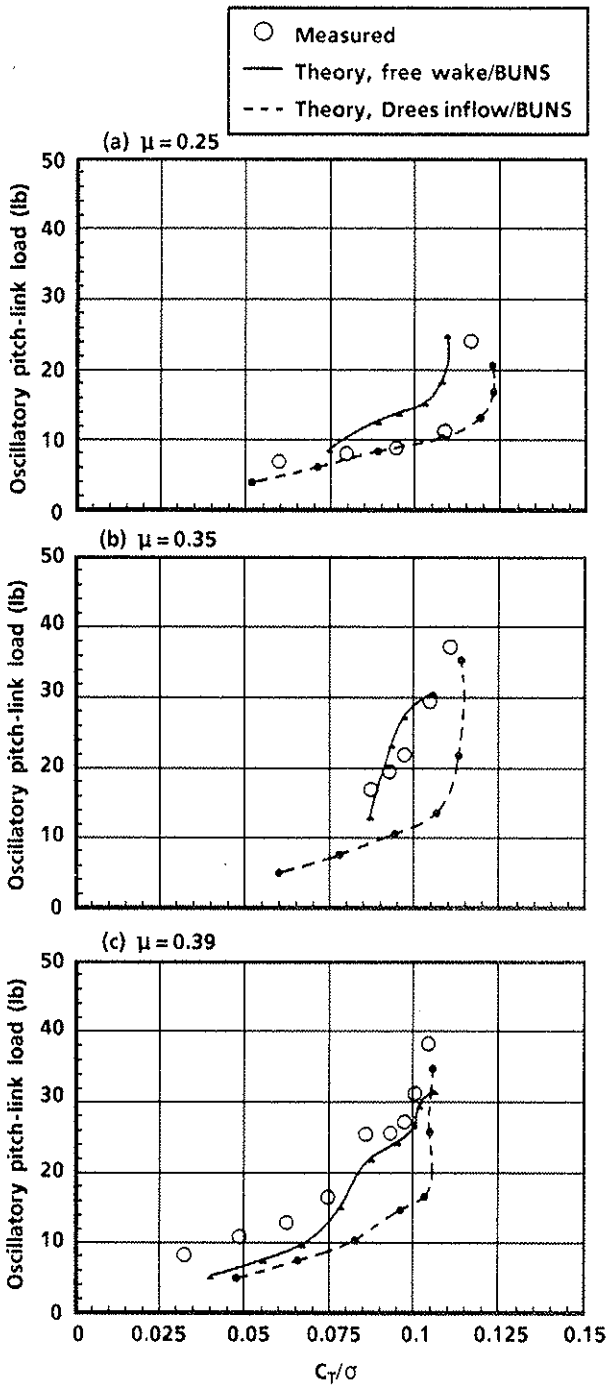

Fig. 5. Correlation of measured and theoretical pitch-link loads for model ALR: baseline blades.

waveforms. Reviewing the data in Figs 13 and 14 leads to the following observations:

1. A nose-down aerodynamic impulse pitching moment resulting from retreating blade simultaneous stall with zero damping produces stall-flutter characteristics.

2. An aerodynamic impulse loading is sufficient to excite all harmonics.

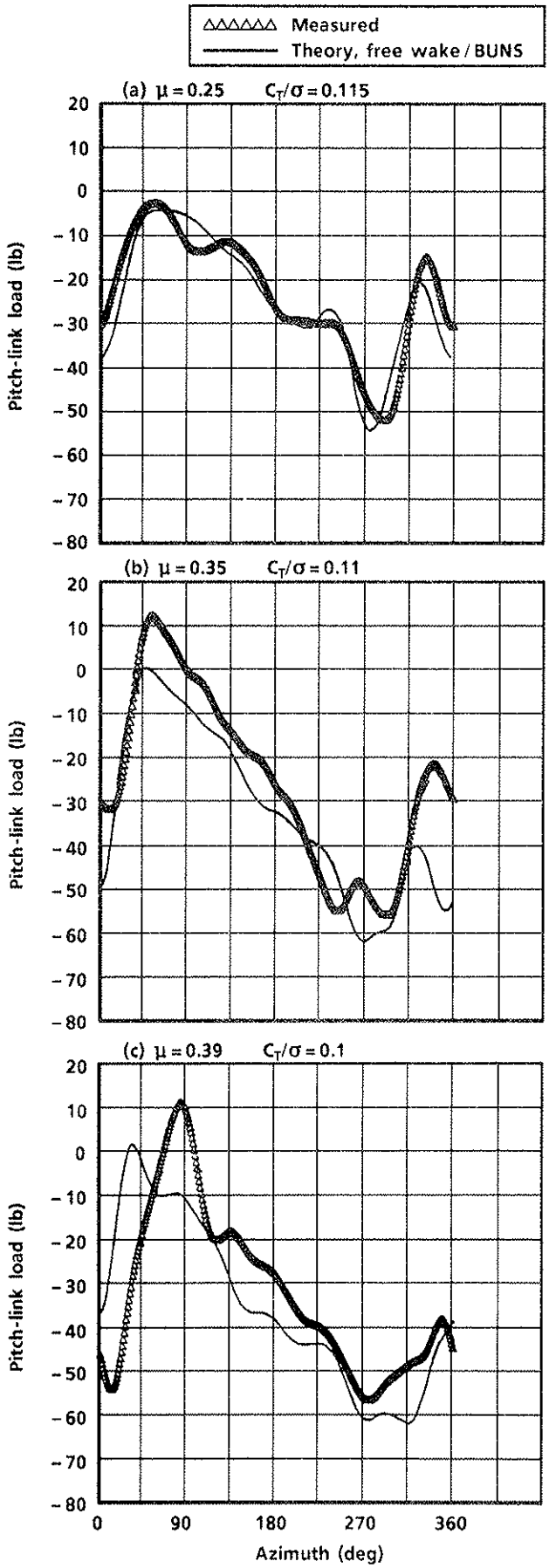

Fig. 6. Correlation of measured and theoretical pitch-link-load waveforms for model ALR: baseline blades.

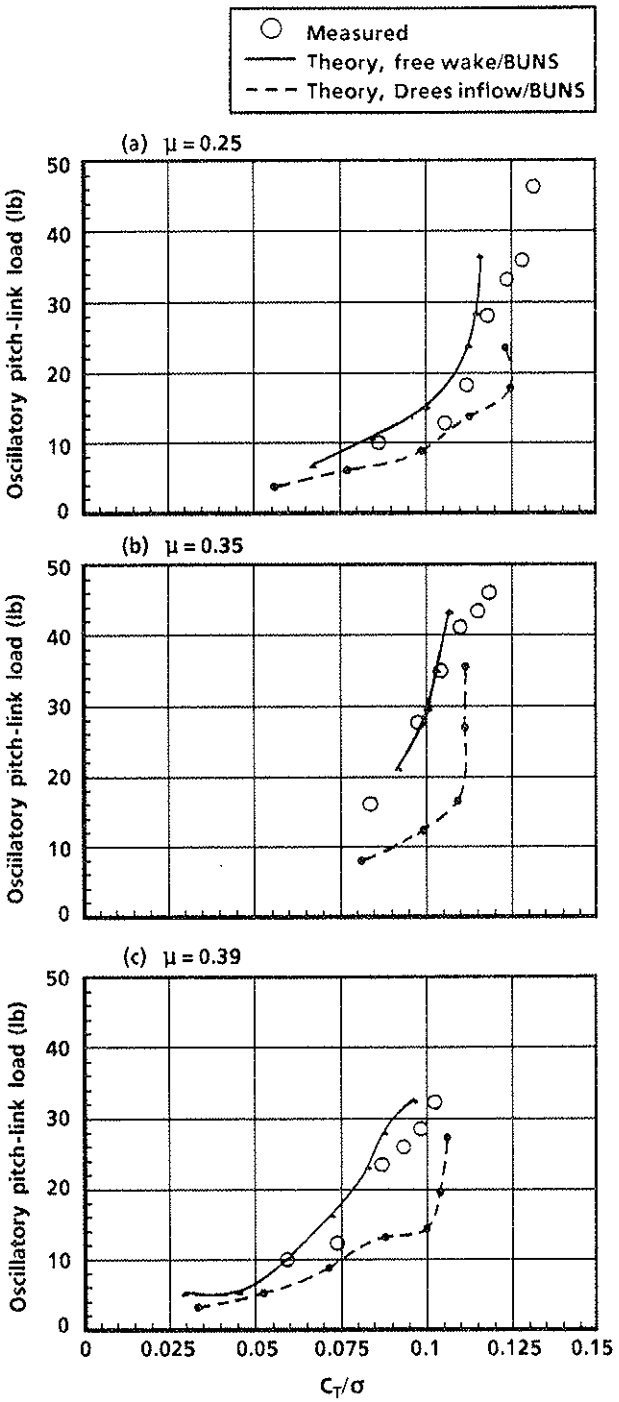

Fig. 7. Correlation of measured and theoretical pitch-link loads for model ALR: torsionally stiff blades.

3. The magnitude of the higher harmonic (3 and above) components depends on the frequency of the torsion mode.

4. With the same aerodynamic excitation, the effect of blade torsional stiffness on overall pitch-link-load response is insignificant.

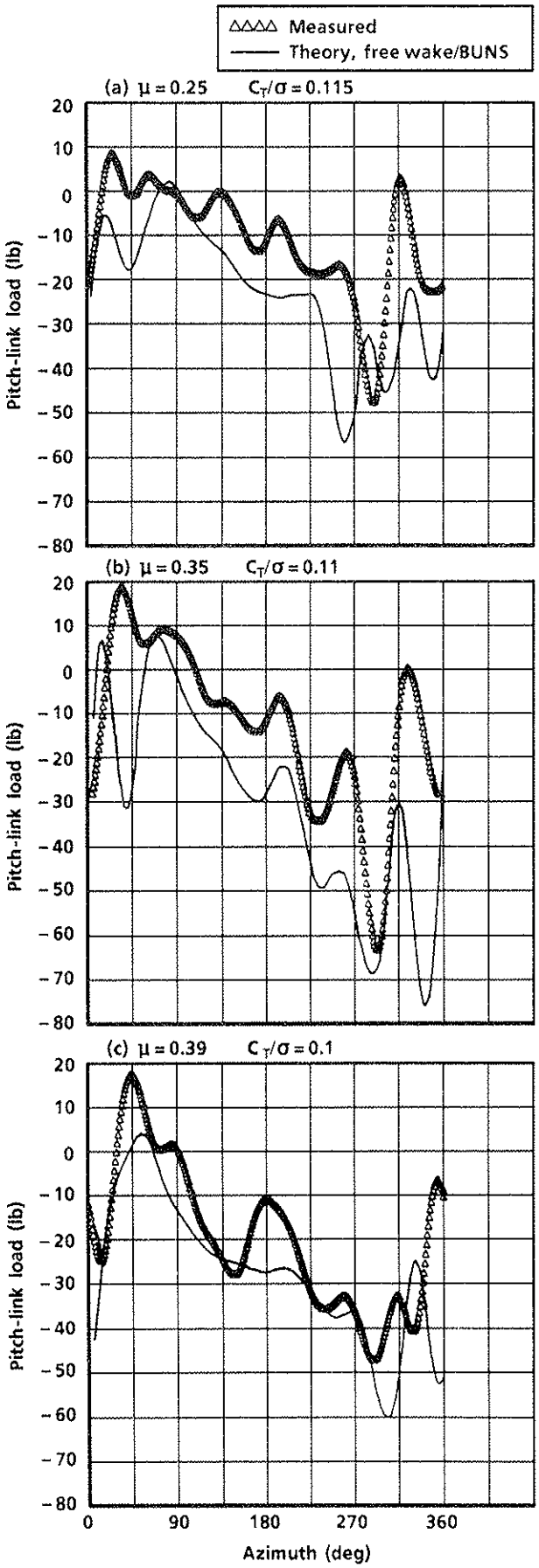

Fig. 8. Correlation of measured and theoretical pitch-link-load waveforms for model ALR: torsionally stiff blades.

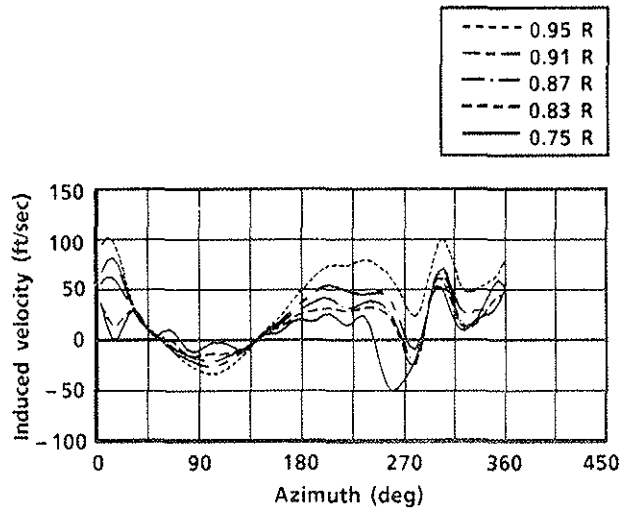

Fig. 9. Prediction of induced velocity for model ALR: torsionally stiff blades, $\mu = 0.35$, $C_T/\sigma = 0.11$.

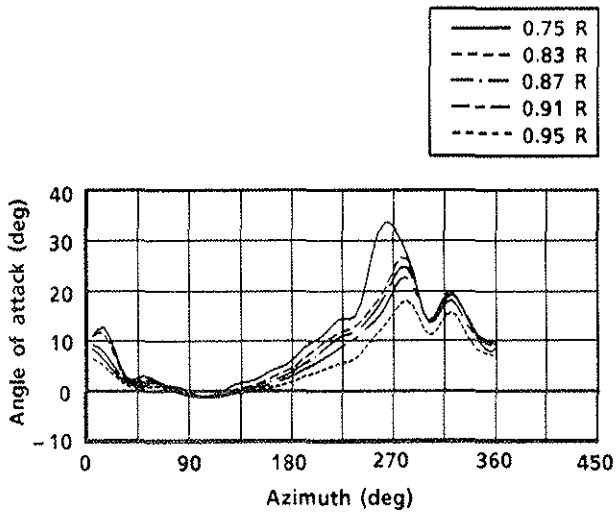

Fig. 10. Prediction of blade angle of attack for model ALR: torsionally stiff blades, $\mu = 0.35$, $C_T/\sigma = 0.11$.

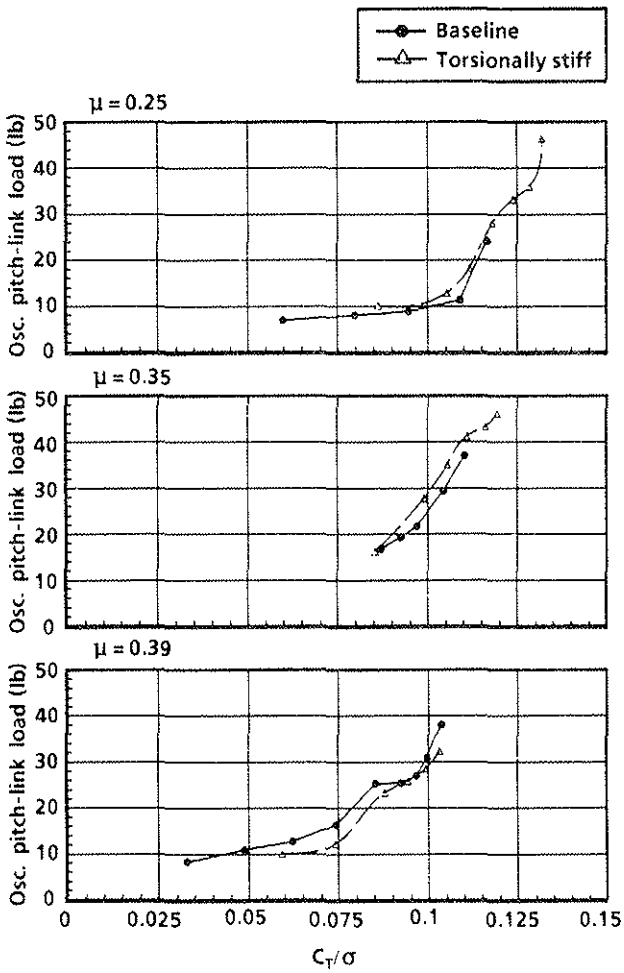

Fig. 11. Comparison of measured pitch-link loads from baseline and torsionally stiff blades on model ALR.

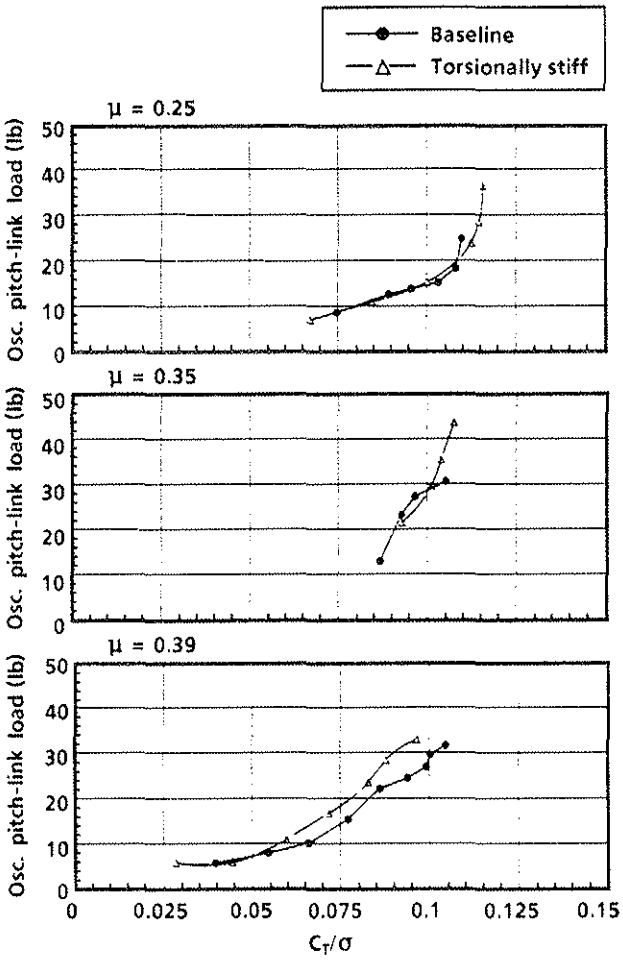

Fig. 12. Comparison of computed pitch-link loads from baseline and torsionally stiff blades on model ALR.

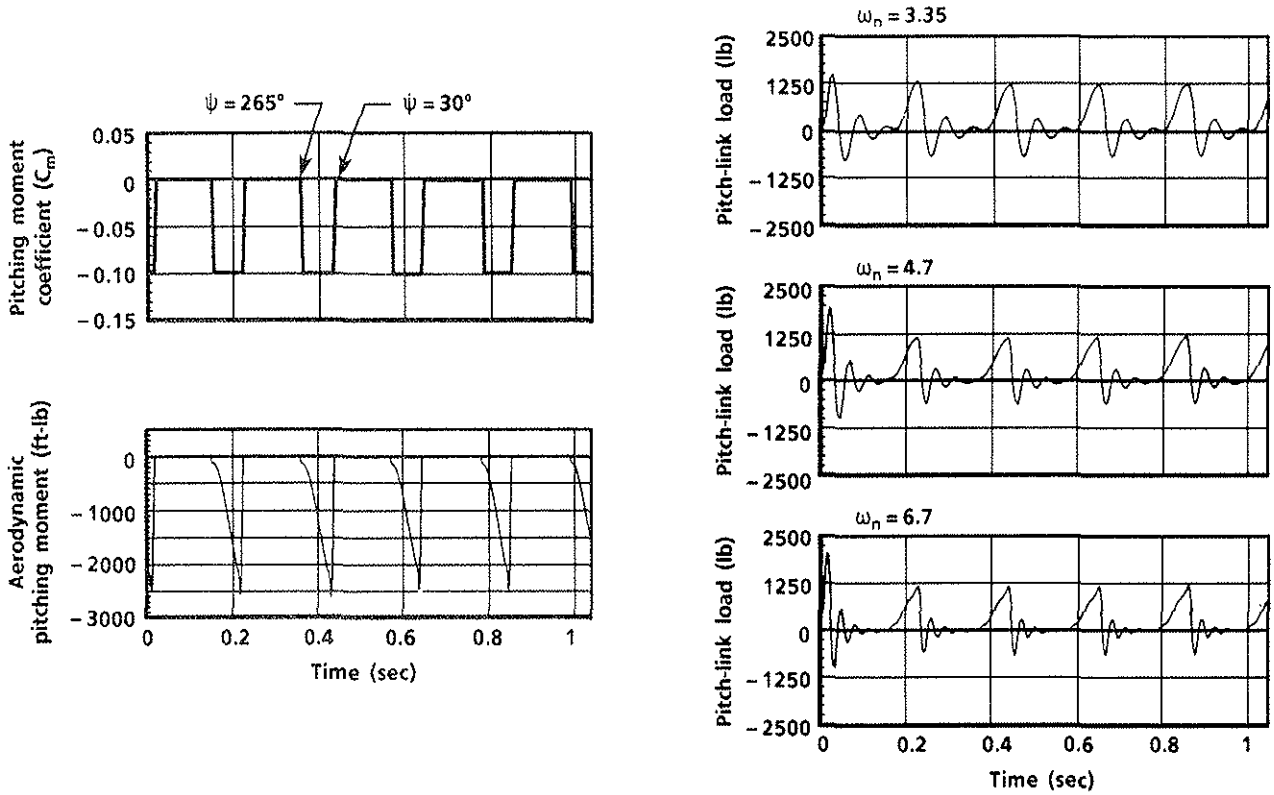

Fig. 13. Pitch-link-load response to an aerodynamic impulse pitching moment.

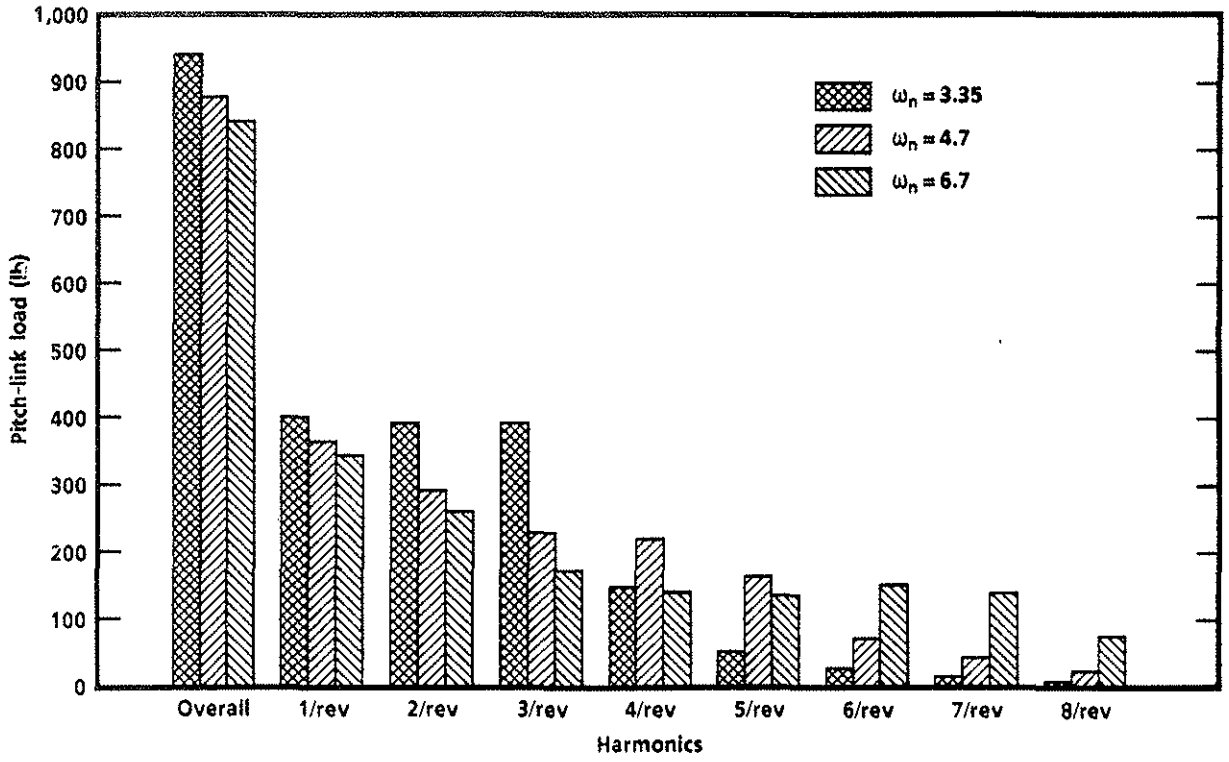

Fig. 14. Harmonic decomposition of pitch-link-load response to aerodynamic impulse pitching moment.

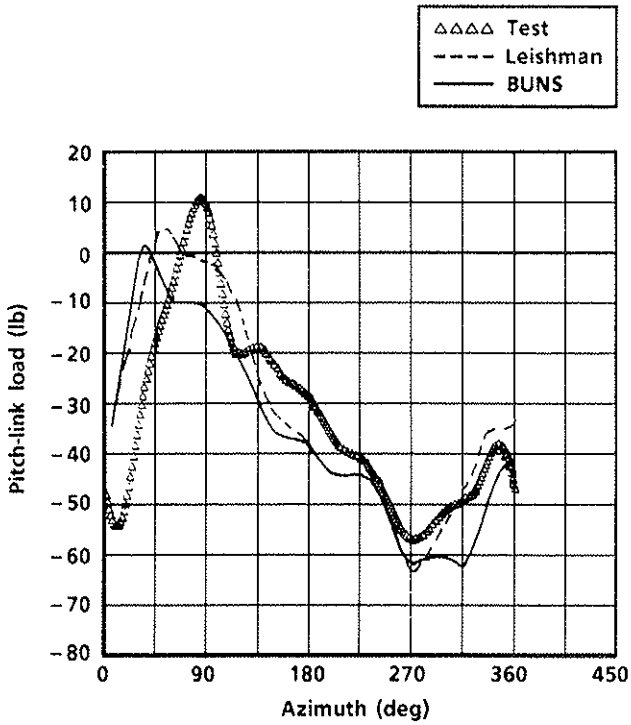

Fig. 15. Correlation of measured pitch-link-load waveforms for model ALR with theory using Leishman and BUNS: baseline blades, $\mu = 0.39$, $C_T/\sigma = 0.10$.

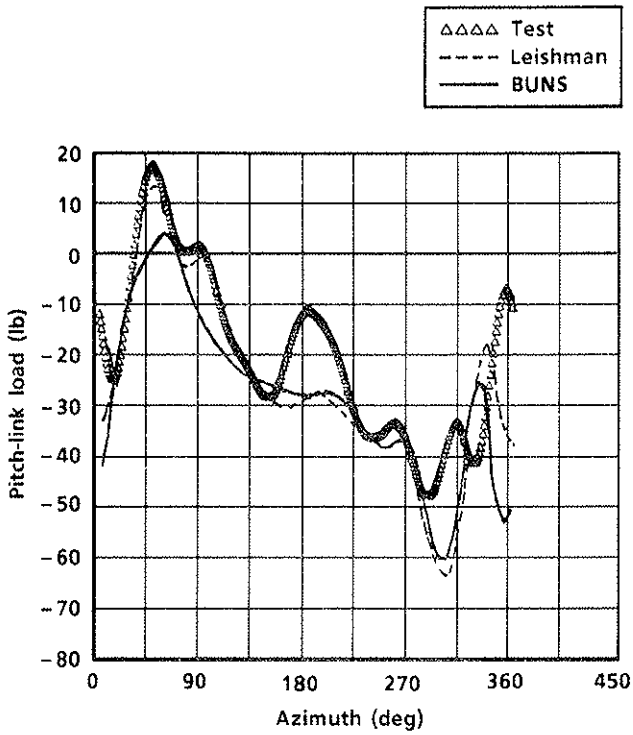

Fig. 16. Correlation of measured pitch-link-load waveforms for model ALR with theory using Leishman and BUNS: torsionally stiff blades, $\mu = 0.39$, $C_T/\sigma = 0.10$.

Effect of Leishman Unsteady Aerodynamics on Pitch-Link Loads

A brief assessment of the effect of Leishman unsteady aerodynamics on pitch-link loads was made using the 1/5 Mach-scaled ALR wind tunnel data. Shown in Fig 15 are pitch-link-load waveforms for the baseline rotor computed with Leishman unsteady aerodynamics and Johnson free wake at $\mu = 0.39$ and $C_T/\sigma = 0.10$. Also shown are measured and BUNS data for comparison purposes. The same comparison is made for the rotor with torsionally stiff blades in Fig 16 for $\mu = 0.39$ and $C_T/\sigma = 0.10$. Based on the limited data in Figs 15 and 16, a slight improvement over BUNS is observed when using Leishman's method. More correlation is needed so that the benefit of using the Leishman unsteady aerodynamics model can be assessed.

Flight Test Correlation

A pitch-link loads analysis using the Johnson free wake model and BUNS unsteady aerodynamics was performed for three full-scale bearingless rotors in maneuvering flight. The three rotors are Bell's ALR (Ref 21), Model 680 (Ref 22), and Model 4BW (Ref 23). The thrust-weighted chord and solidity of the three rotors are 1.55 ft, 0.0992; 1.14 ft, 0.073; and 1.966 ft, 0.1015, respectively. Rotor frequencies of the first four cyclic modes of the three rotors are tabulated in Table 1.

ALR Pitch-Link Loads

Predicted pitch-link loads using the free wake model and BUNS were correlated with flight test data from the ALR during a symmetric pull-up. Results are shown in Fig 17. The theory correlates well in trend and slightly underpredicts the magnitude in high-thrust conditions.

680 Pitch-Link Loads

Predicted pitch-link loads using the free wake model and BUNS were correlated with flight test data from the 680 during a symmetric pull-up. Results are shown in Fig 18. The theory correlates well for high thrust conditions and slightly overpredicts the magnitude for lower thrust coefficients.

4BW Pitch-Link Loads

Correlation data for the 4BW in a symmetric pull-up are depicted in Fig 19. The theory correlates well when the rotor is in deep stall. However, it overpredicts at the lower end of the thrust coefficients. A close examination of harmonic content

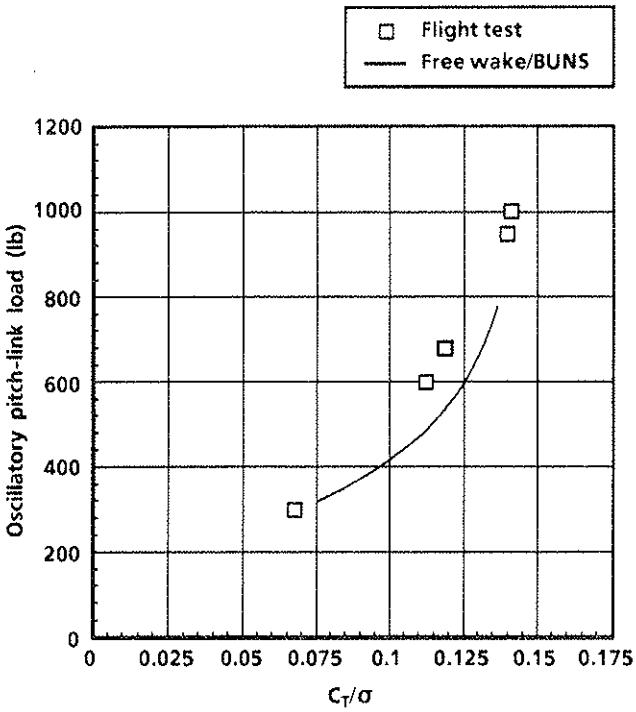

Fig. 17. Correlation of measured and theoretical pitch-link loads in symmetric pull-ups: ALR, μ = 0.28 to 0.31.

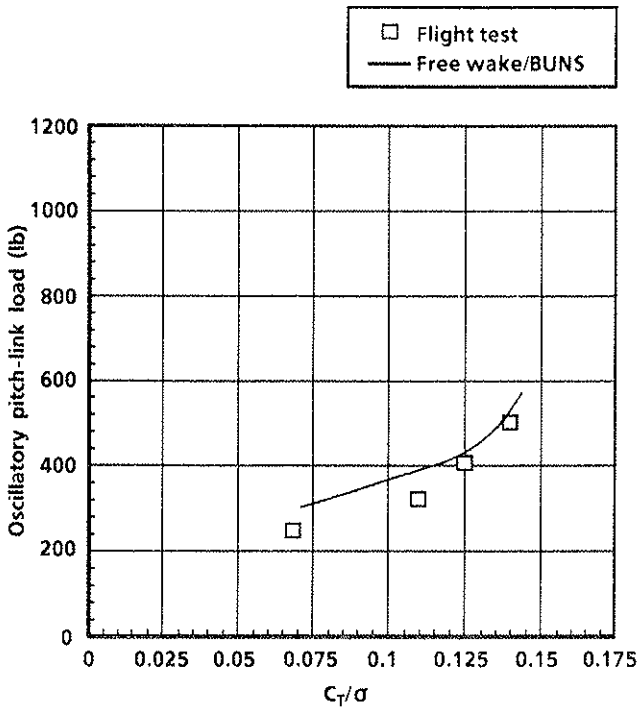

Fig. 18. Correlation of measured and theoretical pitch-link loads in symmetric pull-ups: 680 rotor, μ = 0.28 to 0.31.

of the loads data revealed that the discrepancy was largely due to the overprediction of the 1/rev component. The overprediction was partially attributed to the yoke torsional stiffness representation.

Pitch-Link-Loads Normalization

The measured or predicted pitch-link loads shown in Figs 17, 18, and 19 for the ALR, 680, and 4BW rotors at $\mu \approx 0.3$ have different slopes because the rotors have different solidities and thrust-weighted chords. If the oscillatory pitch-link loads are normalized with respect to solidity and chord-square, the resulting data from the three rotors would fall into a relatively narrow band. Fig 20 shows the measured loads normalized by solidity and chord-square for the three rotors. Notice that the normalized loads have nearly identical slopes, with a slight difference in magnitude. Since the theory correlates well with the measured data (Figs 17, 18, and 19), the characteristics depicted in Fig 20 are also simulated by the analysis.

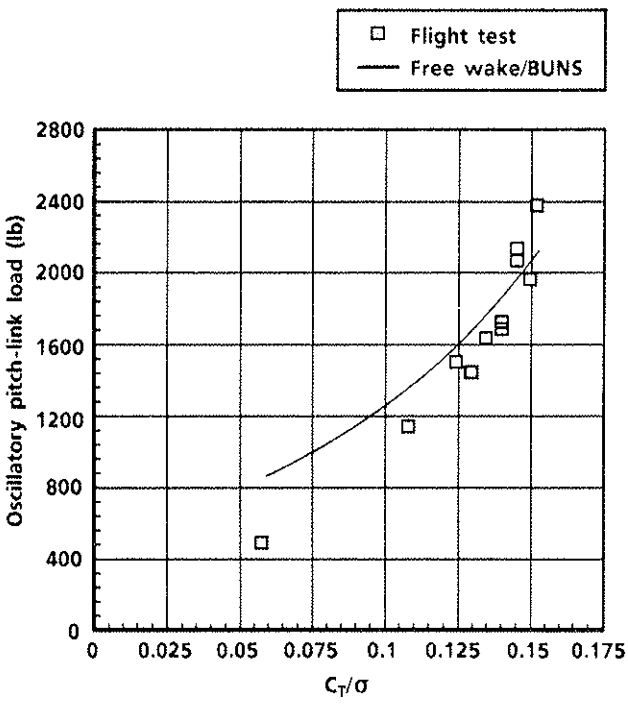

Fig. 19. Correlation of measured and theoretical pitch-link loads in symmetric pull-ups: 4BW rotor, μ = 0.29 to 0.31.

Conclusions

Calculations of pitch-link loads in deep stall were conducted on bearingless rotors using a unified state-of-the-art methodology. The theory was correlated with data measured on five different rotors. Results presented in this paper reveal the following:

1. Strong blade–vortex interaction in deep stall is predicted using the Johnson free wake model.

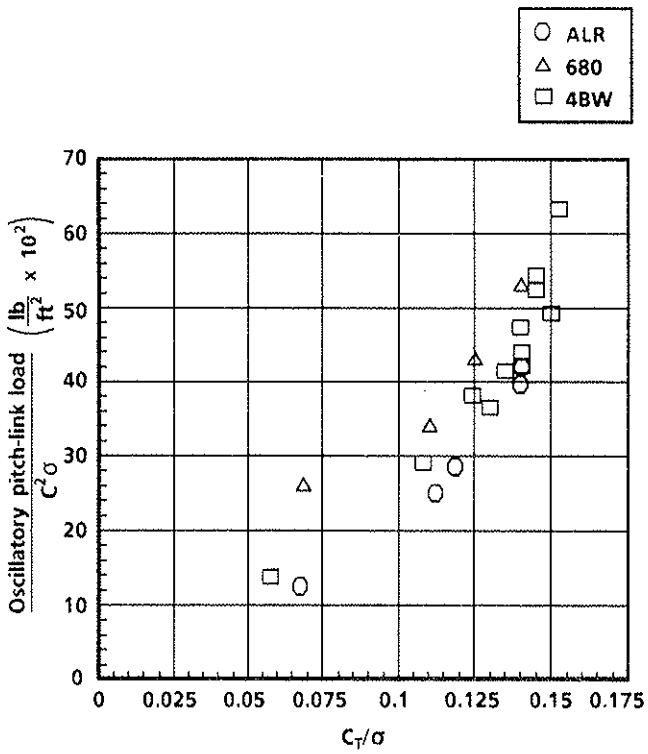

Fig. 20. Comparison of measured ALR, 680, and 4BW pitch-link loads in symmetric pull-ups, normalized by solidity and chord square: μ = 0.28 to 0.31.

2. Blade–vortex interaction contributes significantly to the dynamic stall delay.

3. Both measured data and analytical predictions suggest that the effect of blade torsional stiffness, and hence the torsional frequency, on overall pitch-link-load response is insignificant.

4. Both BUNS and Leishman unsteady aerodynamic models serve well for predictions of pitch-link loads in deep stall.

5. The level of correlation presented in this paper using the COPTER state-of-the-art methodology is encouraging.

References

1. Tarzanin, F. J., Jr., "Prediction of Control Loads Due to Blade Stall," *Journal of the American Helicopter Society*, Vol. 17, (2), April 1972.

2. Scully, M. P., *Computation of Helicopter Rotor Wake Geometry and its Influence on Rotor Harmonic Airloads*, Massachusetts Institute of Technology, ASRL TR 178-1, Mar. 1975.

3. Johnson, W., *Wake Model for Helicopter Rotors in High Speed Flight*, NASA CR 177507, Nov. 1988.

4. Johnson, W., "Calculation of Blade–Vortex Interaction Airloads on Helicopter Rotors," *Journal of Aircraft*, Vol. 26, (5), May 1989.

5. Bousman, W. G., et al., *Correlation of Puma Airloads - Lifting-Line and Wake Calculation*, NASA TM 102212, Nov. 1989.

6. Bousman, W. G., "The Response of Helicopter Rotors to Vibratory Airloads," American Helicopter Society National Specialists' Meeting on Rotorcraft Dynamics, Arlington, TX, Nov. 1989.

7. Harris, F. D., et al., "Rotor High Speed Performance, Theory vs. Test," *Journal of the American Helicopter Society*, Vol. 15, (3), July 1970.

8. Carta, F. O., et al., "Analytical Study of Helicopter Rotor Stall Flutter," American Helicopter Society 26th Annual National Forum, Washington, D.C., June 1970.

9. Gangwani, S. T., "Prediction of Dynamic Stall and Unsteady Airloads for Rotor Blades," *Journal of the American Helicopter Society*, Vol 27, (4), Oct. 1982.

10. Gangwani, S. T., "Development of an Unsteady Aerodynamics Model to Improve Correlation of Computed Blade Stresses with Test Data," 2nd Decennial Specialists' Meeting on Rotorcraft Dynamics, NASA Ames, Nov. 1984.

11. Tran, C. T., and Petot, D., "Semi-empirical Model for the Dynamic Stall of Airloads in View of the Application to the Calculation of Responses of a Helicopter Blade in Forward Flight," Sixth European Rotorcraft and Powered Lift Aircraft Forum, Bristol, England, Sept. 1980.

12. Gaubert, M., and Yamauchi, G. K., "Prediction of SA 349/2 GV Blade Loads in High Speed Flight Using Several Rotor Analysis," American Helicopter Society 43rd Annual National Forum, St. Louis, MO, May 1987.

13. Leishman, J. G, and Beddoes, T. S., "A Generalized Model for Airfoil Unsteady Aerodynamic Behavior and Dynamic Stall Using the Indicial Method," American Helicopter

Society 42nd Annual National Forum, Washington, D. C., June 1986.

14. Leishman, J. G., and Beddoes, T. S., "A Semi-Empirical Model for Dynamic Stall," *Journal of the American Helicopter Society*, Vol. 34, (3), July 1989.

15. Corrigan, J. J., et al., "Developments in Dynamics Methodology at Bell Helicopter Textron," American Helicopter Society 44th Annual National Forum, Washington, D. C., June 1988.

16. Van Gaasbeek, J. R., et al., *Rotorcraft Flight Simulation, Computer Program C81, Volume I - Engineer's Manual*, USARTL TR 77-54A, 1979.

17. Drees, J. M., "A Theory of Airflow Through Rotors and Its Application to Some Helicopter Programs," *Journal of the Helicopter Association of Great Britain*, Vol. 3, (2), July 1949.

18. Schlomach, R. C., and May, J., *Rotor Blade Natural Frequency Analysis for Complex Hub Configuration*, USAAVSCOM TR 85-D-22, July 1989.

19. Wood, T. L., et al., "An Experimental Investigation of Rotor Blade Airloads and Wake Structure at High Advance Ratio," American Helicopter Society 46th Annual National Forum, Washington, D. C., May 1990.

20. McCroskey, W. J., et al., *An Experimental Study of Dynamics Stall on Advanced Airfoil Sections*, Vols 1-3, NASA TM 84245, July 1982.

21. McEntire, K. G., et al., "Flight Test of an Advanced Rotor System for Future Combat Helicopter Applications," American Helicopter Society Specialists' Meeting on Rotary Wing Test Technology, Bridgeport, CT, Mar. 1988.

22. Alsmiller, G. R., et al., "The All-Composite Rotorcraft," American Helicopter Society 39th Annual National Forum, St. Louis, MO, May 1983.

23. Harse, J. H., "The Four-bladed Main Rotor System for the AH-1W Helicopter," American Helicopter Society 45th Annual National Forum, Boston, MA, May 1989.